Biochimica et Biophysica Acta 1798 (2010) 389–400

Contents lists available at ScienceDirect

Biochimica et Biophysica Acta

journal homepage: www.elsevier.com/locate/bbamem

Cell membrane extensions, generated by mechanical constraint, are associated with a sustained lipid raft patching and an increased cell signaling

Romain M. Larive [a,1], Laurent Baisamy [a], Serge Urbach [b], Peter Coopman [a], Nadir Bettache [a,*]

[a] Universités de Montpellier 2 & 1, Centre de Recherche de Biochimie Moléculaire CRBM, CNRS-UMR 5237, 1919 Route de Mende, F-34293 Montpellier cedex 5, France
[b] Institut de Génomique Fonctionnelle, CNRS-UMR 5203, INSERM U661, 141 rue de la Cardonille, F-34094 Montpellier cedex 5, France

ARTICLE INFO

Article history:
Received 4 June 2009
Received in revised form 13 October 2009
Accepted 18 November 2009
Available online 3 December 2009

Keywords:
Lipid rafts
Platelets
Phospholipids
Filopodia
Actin
Mechanical constraint
Cell signaling

ABSTRACT

Platelet activation triggers an imbalance in plasma membrane phospholipids by a specific aminophospholipid outflux, resulting in filopodia formation. Similarly, the addition of a phospholipid excess in the outer leaflet of the plasma membrane induces cellular extensions and actin polymerization. The implication of membrane microdomains in sustaining these mechanical constraints remains, however, unknown and was investigated in human platelets and mouse fibroblasts. The disruption of lipid rafts by cholesterol depletion prevents actin polymerization and formation of cellular extensions. Phospholipid excess triggers raft patching underneath the cell extensions, recruitment of protein raft markers and increase of tyrosine phosphorylation of raft proteins. Using a mass spectrometric analysis of isolated platelet rafts, we identified tyrosine kinases and proteins implicated in the formation of cell membrane extensions, cell adhesion and motility. They are recruited to rafts in response to a mechanical constraint. Taken together, our results demonstrate that exogenous phospholipid addition causes a modulation of the lateral plasma membrane organization and an activation of the cell signaling triggering actin remodeling and the formation of cellular protrusions. Raft disruption abolishes these processes, demonstrating that their integrity is crucial for cell shape changes in response to a mechanical constraint on plasma membrane.

1. Introduction

Plasma membranes of mammalian cells are dynamic structures characterized by the asymmetric transversal distribution of phospholipids between the inner and the outer leaflets [1,2] and by a high lateral mobility of proteins and lipid molecules [3]. The ability of cells to generate regions of membrane curvature is of vital importance in regulating changes in membrane morphology that underlie processes such as membrane trafficking and cell migration [4]. The membrane curvature is generated as a result of a complex interplay between membrane proteins, lipids and physical forces that are applied to the membrane surface. In addition to cytoskeletal proteins, other proteins containing BAR domains (e.g., amphiphysin and endophilin) or MIM homology domains (e.g., IRSp53) contribute to the generation of membrane curvature [5,6]. The shape of a membrane is influenced not only by proteins but also by lipids that could generate the driving forces to produce membrane curvature [7–10]. Like proteins, lipids favor positive curvature (e.g., inverted-cone-shaped lipids), which characterizes the outer leaflet of a membrane bud, or negative curvature (e.g., cone-shaped lipids) as found in the inner leaflet of a bud [11,12]. In fact, during platelet activation, filopodia formation is tightly correlated with the specific aminophospholipid outflux resulting in an excess of phospholipids in the outer leaflet of the plasma membrane [13]. This process is dramatically impaired in the Scott syndrome, a rare congenital bleeding disorder, in which aminophospholipid outflux is disturbed [14]. Similarly, the incorporation of a lipid directly into one monolayer induces an asymmetry of monolayer areas and thereby increases the intrinsic curvature of the whole bilayer, causing a curling of the membrane away from the side to which the lipid is added, thus expanding the monolayer with more lipids and compressing the monolayer with less lipids [8–10,15–17]. To support the exerted forces, it is hypothesized that the areas of membrane interacting with the cytoskeleton have a specific lipid composition. These areas are enriched with cholesterol and sphingolipids and form the so-called membrane microdomains, also known as detergent-resistant membranes (DRMs) or lipid rafts [18]. Experiments with different cell types show, however, that DRM composition does not always perfectly represents raft composition [19,20]. Recent studies have suggested that lipid rafts are implicated in supporting membrane curvature [7] and their properties are strongly influenced by line tension [21]. Indeed, the lipid rafts are intimately linked to curved membranes and are concentrated in filopodia [22,23].

Abbreviations: PS, phosphatidylserine; PC, phosphatidylcholine; PE, phosphatidylethanolamine; PL, phospholipids; MβCD, methyl beta cyclodextrin; DRMs, detergent-resistant membranes

* Corresponding author. Tel.: +33 4 67 14 47 25; fax: +33 4 67 14 47 27.
E-mail addresses: romain.larive@usal.es (R.M. Larive), nadir.bettache@univ-montp2.fr (N. Bettache).
[1] Present address: Centro de Investigacion de Cancer and Instituto de Biologia Molecular del Cancer, University of Salamanca, E37007 Salamanca, Spain.

0005-2736/$ – see front matter © 2009 Elsevier B.V. All rights reserved.
doi:10.1016/j.bbamem.2009.11.016

Our previous studies showed that the addition of low amounts of short-chain analogues of phospholipids (1–2% of endogenous phospholipids) into the outer leaflet of human resting platelets or mouse fibroblast plasma membrane induces the formation of cell membrane extensions, such as long filopodia and lamellipodia, and reversible actin polymerization [15]. We demonstrated that a fraction of PI-3-kinase is reversibly activated and recruited to the plasma membrane and that Akt is partially phosphorylated by this small phospholipid excess in the outer leaflet of the plasma membrane of resting platelets. The formation of cellular protrusions is inhibited by two unrelated PI-3-kinase inhibitors, wortmannin and LY294002, and by the inhibition of actin polymerization with cytochalasin D. It is well established that lateral assembly of glycosphingolipids and cholesterol in membrane microdomains form platforms for numerous cellular events, including membrane trafficking, cell signaling and adhesion [18]. Lipid rafts are resistant to solubilization by non-ionic detergents, such as Triton X-100 at low temperature, and can be isolated by density gradient ultracentrifugation due to their low buoyant density. Many proteins involved in signal transduction co-purify with lipid rafts isolated on sucrose gradients. These include proteins attached to the outer surface of the plasma membrane, such as glycosyl phosphatidylinositol (GPI)-linked proteins (CD59, PLAP) [24–26] and many dual acylated cytoplasmic proteins attached to the inner face of the plasma membrane, such as the Src family kinases Lck, Fyn, Lyn [27–29].

In the present work, we attempted to determine the implication of membrane microdomains in sustaining the mechanical constraint induced by the addition of excess phospholipid on the outer leaflet of plasma membrane. Microscopic, biochemical and proteomic approaches were performed to explore the membrane dynamics and the mechanism of cell shape changes in response to a mechanical constraint acting on the plasma membrane. Using these approaches, we demonstrate that lipid rafts play a crucial role in the formation of cellular extensions, in actin polymerization and in triggering cell signaling in response to a mechanical constraint applied to resting human platelets and L929 mouse fibroblasts.

2. Materials and methods

2.1. Preparation of human platelets

Blood collected in 0.15 vol. of ACD buffer containing 85 mM trisodium citrate, 111 mM dextrose, 71 mM citric acid, was obtained from healthy volunteers. Platelets were prepared at room temperature using the erythrocyte cushion procedure, as previously described [30,31]. After staining with Plaxan reagent (Sobioda SA, France) and counting, platelets were gently resuspended in Bevers buffer containing 96 mM NaCl, 1 mM $CaCl_2$, 2.7 mM KCl, 2 mM $MgCl_2$, 5 mM dextrose, 50 mM HEPES, pH 7.4 at 2.2×10^9 platelets/ml. Platelets were incubated for 30 min at 37 °C (pH 7.4) before treatments. Platelets were optionally activated at 37 °C by adding 1 IU/ml thrombin for 2 min in the presence of 1 mM external Ca^{2+} (pH 7.0).

2.2. Cell culture

L-929 mouse fibroblasts (CCL-1; American Type Culture Collection) were grown in RPMI 1640 with glutamax (GIBCO BRL) supplemented with 10% fetal bovine serum, 25 IU/ml penicillin and 25 μg/ml streptomycin (GIBCO BRL) at 37 °C in the presence of 5% CO_2. They are used at ~80% confluence. For microscopy, cells were plated onto coverslips coated with poly-L-lysine and human fibronectin (Sigma Chemical Co.). For poly-L-lysine coating, coverslips were incubated on a drop of aqueous 100 μg/ml poly-L-lysine for 30 min at room temperature, washed with distilled water and air dried. Fibronectin was coated onto poly-L-lysine-treated coverslips by incubation on a drop of 25 μg/ml fibronectin in PBS at 4 °C overnight. After rinsing in PBS, these coverslips were used without drying.

2.3. Nocodazole treatment

Microtubules were depolymerized according to the method of Kaverina and collaborators [32]. Briefly, L-929 fibroblasts were trypsinized and resuspended in fresh culture medium containing 2.5 μg/ml nocodazole (Sigma Chemical Co.). Cells were immediately plated onto coverslips or culture dishes for 3 h at 37 °C in the presence of 5% CO_2.

2.4. Incubation of L929 fibroblasts and resting platelets with phospholipid analogues

L929 fibroblasts pre-treated with nocodazole (and in some cases with MβCD) were rinsed twice in PBS and incubated with 50 μM dilauroyl-phosphatidylcholine (DLPC; Sigma Chemical Co.) or a short-chain spin-labeled phosphatidylserine (PS; [33]) in serum-free medium for 2 min at room temperature with gently shaking. Platelets at 2.2 10^9 cells/ml pre-treated or not with MβCD were incubated at 37 °C without shaking with PC or PS analogues at 1% of total phospholipids as previously described [33]. After 2 and 30 min, phospholipid incubation was stopped for further analysis.

2.5. Determination of actin filament content in platelets

Platelets were lysed by the addition of an equal volume of buffer containing 2% Triton X-100, 10 mM EGTA and 100 mM Tris–HCl, pH 7.4. The actin filament content was determined by DNase-I inhibition assay as described previously [34,35]. Data from three independent experiments represent the mean ± SEM. Student's *t* test was used for statistical analysis. DNA and DNase-I were obtained from Sigma Chemical Co.

2.6. Scanning electron microscopy (SEM)

Platelets were prepared as reported previously [31]. Briefly platelets were fixed with 2% glutaraldehyde in a 0.1-M cacodylate solution, pH 7.4, for 30 min at 4 °C and then treated with 1% osmium tetroxide in a 30-mM sodium acetate, 30 mM sodium veronal and 0.02 N HCl buffer. Thereafter, platelets were washed in distilled water and allowed to sediment onto Thermanox coverslips (Nunc Inc.). Samples were dehydrated through a graded alcohol series. After drying by using the CO_2 critical point method and coating with gold, samples were observed on a Jeol 6300F microscope. Photos were assembled using Photoshop (Adobe) and PowerPoint (Microsoft).

2.7. Raft disruption

L-929 mouse fibroblasts previously pre-treated or not with nocodazole were rinsed once in PBS and incubated with 5 mM MβCD (Methyl-β-cyclodextrin; Sigma Chemical Co.) in serum-free medium for 30 min at 37 °C in the presence of 5% CO_2. Fibroblasts were washed twice with PBS for removing MβCD-cholesterol complexes. For platelets raft disruption, they were incubated with 5 mM MβCD in Bevers buffer for 10 min at 37 °C, spun at 6000 ×*g* for 3 min and resuspended in Bevers buffer with or without addition of phospholipid analogues.

2.8. Raft patching in L-929 fibroblasts and platelets

Raft patching was performed after 8 μg/ml biotin-conjugated cholera toxin B subunit (Sigma Chemical Co.) incubation in TBS with 0.1% BSA for 30 min at 12 °C, followed by rhodamine-conjugated streptavidin (Sigma Chemical Co.) 1:100 in TBS with 0.1% BSA treatment for 30 min on ice. Platelets were pre-treated or not with MβCD (5 mM for 10 min), incubated with DLPC (1% of total PLs for

2 min) and fixed for 30 min with 2% paraformaldehyde in PBS at room temperature. Surface plasma membrane GM1 was detected by biotinylated cholera toxin followed by incubation with fluorescein-conjugated Streptavidin.

2.9. Microscopy

For phase-contrast microscopy, L-929 fibroblasts were treated as described above and fixed for 30 min with 2% paraformaldehyde in PBS at room temperature. Cells were washed three times with Tris-buffered saline (TBS) and three times with distilled water. Coverslips were mounted with Mowiol and allowed to polymerize at 4 °C overnight. Preparations were observed on a LEICA DMRA2 microscope, using a 40× oil objective. Data were acquired using a cooled CCD camera (Photometrics Coolsnap HQ) driven by Metamorph software. For DIC and epifluorescence microscopy, platelets were pretreated as described above. Observations were performed with a Zeiss Axioimager microscope using AxioVision software for images acquisition and processing.

2.10. Confocal microscopy

Cells were fixed and washed with TBS as for phase-contrast microscopy. Non-specific sites blocking and cell permeabilization were achieved by incubation for 30 min with 1% gelatin, 0.03% saponin in TBS at room temperature. Cells were rinsed once with 0.2% gelatin, 0.03% saponin in TBS and incubated with appropriate molecules. For actin labeling, 0.5 μM TRITC-conjugated phalloidin in a buffer containing 20 mM KH_2PO_4, 10 mM PIPES, 5 mM EGTA, 2 mM $MgCl_2$ and 0.03% saponin for 30 min was used. For detecting tyrosine-phosphorylated proteins, we used 4G10 hybridoma supernatant for 30 min followed by TRITC-conjugated donkey anti-mouse antibody. For GM1 detection, we used 8 μg/ml FITC-conjugated cholera toxin B subunit (Sigma Chemical Co.) for 30 min. Coverslips were washed three times with 0.2% gelatin, 0.03% saponin in TBS between antibody incubations. Preparations were observed on a LEICA TCS 4D confocal laser scanning microscope, using a 40× oil objective. Data were acquired using cooled CCD camera (Hitachi KP-161) driven by Scanware software.

2.11. Raft isolation from L-929 fibroblasts and resting platelets

L-929 fibroblasts treated or not with different reagents ($5–6\times10^6$ cells) were lysed by adding 4 ml of ice-cold buffer containing 1% Triton X-100, 25 mM Tris–HCl, 150 mM NaCl, 5 mM EDTA, pH 7.5, 50 mM NaF, 1 mM Na_3VO_4, protease inhibitor cocktail (Boehringer Mannheim) in culture dishes. Cells were immediately scrapped, harvested and incubated 20 min on ice. Alternatively, resting platelets (4.4×10^9 cells) were lysed by the addition of an equal volume of buffer containing 2% Triton X-100, 10 mM EGTA and 100 mM Tris–HCl, pH 7.4, 100 mM NaF, 2 mM Na_3VO_4, protease inhibitor cocktail (Boehringer Mannheim). The lysate was homogenized with 10 strokes of a Dounce homogenizer. Subsequent procedures were performed at 4 °C. The total lysate was adjusted to 40% sucrose (in lysis buffer without Triton) and placed in the bottom of Ultraclear ultracentrifuge tubes (Beckman Dickinson). Four-milliliter samples of 30% sucrose (in lysis buffer without Triton) and 1.5 ml of lysis buffer without Triton were poured above the 40% sucrose layer. Gradients were spun for 16 h, 4 °C at 39,000 rpm ($192,000\times g$) in a Beckman SW40Ti rotor. Fractions of 1 ml were collected from the top and were diluted 6-fold with buffer containing 25 mM Tris–HCl, 150 mM NaCl and 5 mM EDTA, pH 7.5, to reduce sucrose concentration. Diluted fractions were spun for 1 h, 4 °C at 39,000 rpm ($100,000\times g$) in a Beckman 50Ti rotor. After removing supernatant, Triton insoluble material was solubilized in 1× electrophoresis sample buffer.

2.12. Gel electrophoresis and immunoblotting

Proteins were separated on SDS–PAGE (10%) and detected with Colloidal Brilliant Blue G reagent (Sigma Chemical Co.) or transferred onto PVDF membranes (Immobilon P, Millipore, Bedford, MA). Non-specific binding of proteins to the membrane was blocked with TBS containing 0.05% Tween-20 (TTBS) and 5% BSA for 1 h at room temperature. Tyrosine-phosphorylated protein staining was performed using 4G10 hybridoma supernatant (1:10 in TTBS with 1% BSA) for 1 h. CD36 and flotillin-1 were revealed with monoclonal anti-CD36 antibody (Cat No. 0765, Immunotech) used at 1:1000 and with monoclonal anti-flotillin-1 antibody (Cat No 610821, BD Biosciences) used at 1:100. The membranes were then incubated with horseradish peroxidase-conjugated goat anti-mouse antibody. After three washes with TTBS, the proteins were visualized using ECL detection reagents and X-ray film according to the supplier's instructions. The ganglioside GM1 was revealed by dot blot with biotin-conjugated cholera toxin B subunit followed by incubation with horseradish peroxidase-conjugated streptavidin.

2.13. In-gel digestion and MS analysis of platelet raft proteins

The proteins from 2 to 4 top fractions of Triton insoluble materials were pooled and separated by 4–15% gradient SDS–PAGE. The gel was stained with the Colloidal Brilliant Blue G reagent (Sigma) according to the supplier's instructions. Protein bands were cut and in-gel digested using trypsin (sequencing grade; Promega, Charbonnières, France) as described [36]. Digested proteins were dehydrated in a vacuum centrifuge, solubilized in 3 μl of formic acid (2%). Samples (1 μl) were analyzed online on an ESI quadrupole time-of-flight (Q-TOF) mass spectrometer (QSTAR Pulsar-i, Applied Biosystems, Foster City, CA) coupled with an Ultimate 3000 HPLC (Dionex, Amsterdam, Netherlands). Desalting and pre-concentration of samples were performed on-line on a Pepmap® precolumn (0.3 mm × 10 mm). A gradient consisting of 0–40% B in 60 min and 40–80% B in 15 min (A = 0.1% formic acid, 2% acetonitrile in water; B = 0.1% formic acid in acetonitrile) at 300 nl/min was used to elute peptides from the capillary (0.075 × 150 mm) reverse-phase column (Pepmap®, Dionex). The Q-TOF was fitted with an uncoated silica PicoTip Emitter (NewOjective, Woburn, USA) with an outlet diameter of 8 μm. Spectra were recorded using the Analyst QS 1.1 software (Applied Biosystems). Parameters were adjusted as follows: ion spray voltage (IS), 1800 V; curtain gas (CUR), 25; declustering potential (DP), 75 V; focusing potential (FP), 265 V; and declustering potential 2 (DP2), 15 V. Spectra were acquired with the instrument operating in the information-dependent acquisition mode throughout the HPLC gradient. Every 7 s, the instrument cycled through acquisition of a full-scan spectrum (1 s) and two MS/MS spectra (3 s each). Peptide fragmentation was performed using nitrogen as collision gas (CID) on the most abundant doubly or triply charged ions detected in the initial MS scan, with a collision energy profile optimized according to peptide mass (using manufacturer parameters) and an active exclusion time of 0.60 min. All MS/MS spectra were searched against the Homo sapiens entries of either SwissProt or TrEMBl databases (Unitrop 10.2, http://www.expasy.ch) by using the Mascot v 2.1 algorithm (http://www.matrixscience.com). Identification was done on the basis of at least one specific peptide. All significant hits ($p<0.05$) were manually inspected.

3. Results

3.1. Lipid raft integrity is necessary for PL excess-induced actin rearrangement in resting platelets

We have already shown that the addition of small amount (1–2% of total phospholipids) of short-chain phospholipid analogues to the

outer leaflet of plasma membrane of resting human platelets or to L929 fibroblasts generates reversible filopodia and plasma membrane extensions [15]. The added phospholipid analogue is uniformly distributed in the outer leaflet of the plasma membrane. We have shown that filopodia formation in platelets induced by thrombin or Ca^{2+}-ionophore A23187 (which triggers platelet activation) or by PC (which does not trigger platelet activation) was inhibited by cytochalasin D (an inhibitor of actin polymerization) but not nocodazole (a microtubule disrupting agent that did not induce serotonin secretion). According to this observation, filamentous actin quantification by DNase-I inhibition assay revealed that phospholipid excess induced actin polymerization in a PI 3-kinase-dependent manner [15]. In this study, we show that the disruption of lipid rafts by cholesterol depletion in resting human platelets prevents filopodia formation, as observed by scanning electron microscopy (Fig. 1A), and prevents actin polymerization and remodeling, as showed by DNase-I inhibition assay (Fig. 1B). Cholesterol depletion by methyl-β-cyclodextrin (MβCD) in resting human platelets did interfere neither with the cell morphology (Fig. 1A, MβCD) as compared to the control (Fig. 1A, Ctrl) nor with the F-actin content (Fig. 1B, MβCD) as compared to the control (Fig. 1B, Ctrl). However, the cholesterol depletion before the addition of phospholipid excess to the outer leaflet inhibits filopodia formation (Fig. 1A, MβCD + PC) as compared to resting platelets incubated with phospholipid excess without cholesterol depletion (Fig. 1A, PC). In the same manner, actin polymerization induced by phospholipid excess (Fig. 1B, PC) was completely abolished in resting platelets pre-treated with MβCD before phospholipid addition (Fig. 1B, MβCD + PC). Taken together, these data indicate that cholesterol and lipid raft integrity are important for platelet response (filopodia formation and actin

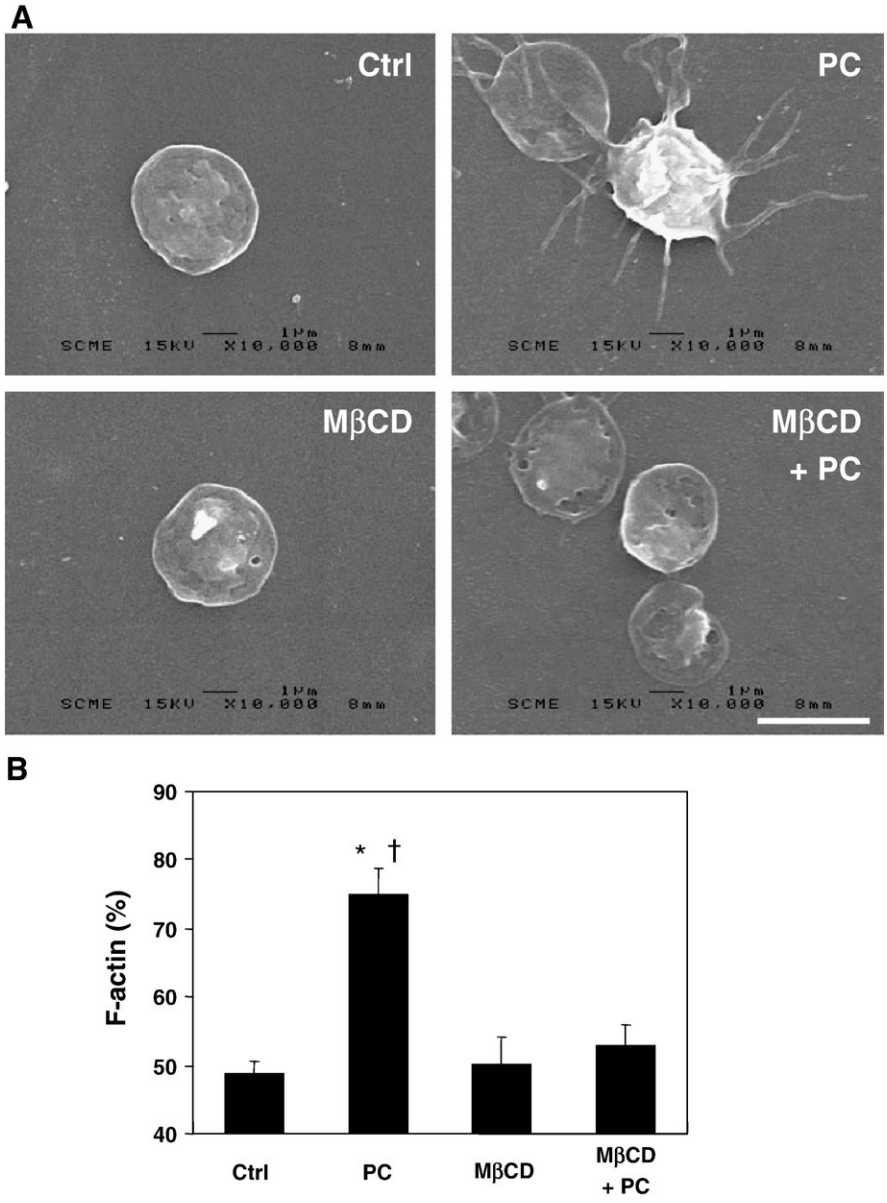

Fig. 1. Implication of cholesterol in filopodia extension and actin polymerization induced by a phospholipid excess in the platelet plasma membrane. (A) Scanning electron micrographs showing the representative morphology of resting platelets (CTRL); platelets incubated with phosphatidylcholine (PC) for 2 min; resting platelets pre-treated with methyl beta cyclodextrin (MβCD); platelets pre-treated with MβCD and then incubated with PC 2 min (MβCD + PC). Micrographs are representative for the cells from at least three independent experiments. Scale bar, 3 μm. (B) Induction of actin polymerization by excess phospholipids in resting platelets. Actin filament content in different platelet extracts was determined by the DNase 1 inhibition assay as indicated in the Materials and methods section. Ctrl, the actin filament content in resting platelets; PC, the actin filament content in platelets incubated with PC for 2 min; MβCD, the actin filament content in resting platelets treated with MβCD; MβCD + PC, the actin filament content in platelets pre-treated with MβCD before their incubation with PC for 2 min. Error bars indicate SEM ($n = 3$). *$p < 0.01$ vs. CTRL; †$p < 0.01$ vs. MβCD + PC.

polymerization) to a mechanical constraint imposed by a phospholipid excess.

3.2. Lipid rafts concentrate underneath the cellular extensions induced by a phospholipid excess in fibroblasts

To visualize lipid rafts in L929 fibroblasts submitted to a mechanical constraint, cells were plated onto coverslips coated with poly-L-lysine and fibronectin. To remove pre-existing cellular extensions involved in cell adhesion and locomotion, fibroblasts were treated with nocodazole, which depolymerizes microtubules [32]. The nocodazole-treated fibroblasts are shown in Fig. 2 (Noco) and the control fibroblasts are shown in Fig. 2 (Ctrl). The cells were then incubated with a phospholipid excess (Fig. 2A, Noco + PC). Alternatively, the cholesterol of the plasma membrane was first depleted by incubating the cells with MβCD (Fig. 2A, Noco + MβCD + PC). The fibroblasts were fixed without permeabilization and the GM1 ganglioside raft marker was patched with biotin-conjugated cholera toxin B subunit and revealed with rhodamine-conjugated streptavidin. The cells were observed with phase-contrast and fluorescence microscopy. In this experiment, the mechanical constraint caused by the addition of an excess of phospholipids induces cellular extensions in nocodazole-treated fibroblasts and the GM1 lipid raft marker forms punctuate sites in the plasma membrane sustaining the membrane extensions (Fig. 2A, Noco + PC). However, when the cholesterol was depleted, the membrane extensions induced by a phospholipid excess were impaired and GM1 was homogeneously distributed all over the plasma membrane (Fig. 2A, Noco + MβCD + PC) in the same manner as the nocodazole-treated fibroblasts without any other treatment (Fig. 2A, Noco). We performed the same experiment with platelets (Fig. 2B). The addition of phospholipids induces formation of filopodia in which the raft marker GM1 is localized (Fig. 2B, PC). The formation of filopodia and the GM1 localization in filopodia were abolished by MβCD treatment (Fig. 2B, MβCD + PC).

These results indicate that the lipid raft integrity is essential for the fibroblast response to a mechanical constraint and that lipid rafts accumulate underneath the cellular extensions after addition of excess phospholipid to the outer leaflet of fibroblast and platelet plasma membrane.

3.3. Mechanical constraint triggers actin remodeling and protein tyrosine phosphorylation in cellular extensions of fibroblasts via lipid rafts

To investigate the consequences of a mechanical constraint on the actin cytoskeleton and the protein tyrosine phosphorylation in L929 fibroblasts, we incubated these cells with phospholipid excess. Implication of lipid rafts in these responses is tested by a prior cholesterol depletion. To detect F-actin and tyrosine-phosphorylated proteins, cells were permeabilized with saponin that does not affect the clustering of the ganglioside GM1 as we obtained a staining of the cytosol and nearby cell membrane extensions (Fig. 3B, Noco + PC). Induced membrane extensions are maintained as evidenced by a strong actin polymerization (Fig. 3A, Noco + PC) and are enriched in tyrosine-phosphorylated proteins (Fig. 3B, Noco + PC). These membrane extensions, the actin remodeling and the enhanced tyrosine phosphorylation are dependent of the integrity of lipid rafts. Indeed, treatment with MβCD prevents membrane extensions, actin polymerization (Fig. 3A, Noco + MβCD + PC), tyrosine phosphorylation and GM1 clustering (Fig. 3B, Noco + MβCD + PC). Our results demonstrate that lipid rafts play a crucial role in phospholipid

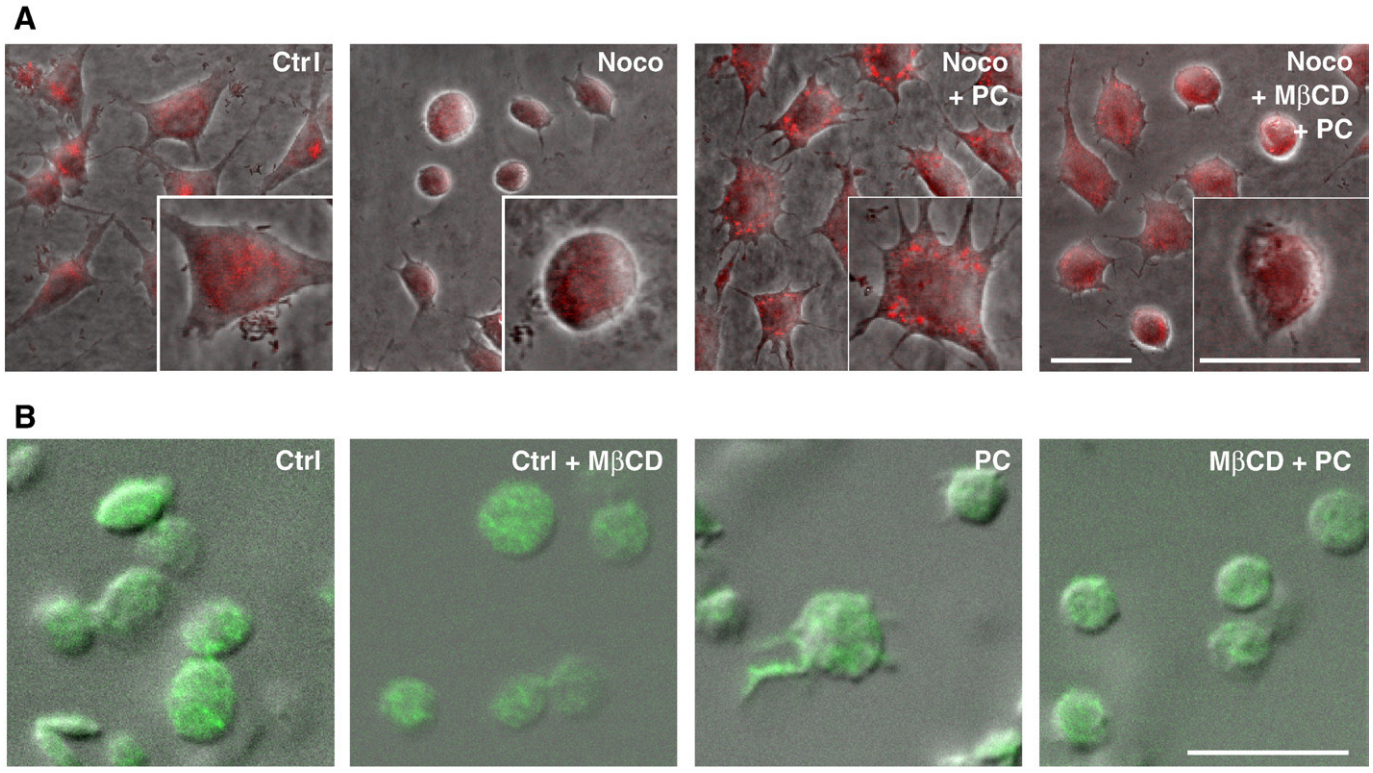

Fig. 2. Patching of lipid rafts underneath the plasma membrane extensions induced by a phospholipid excess in fibroblasts and platelets. (A) Merge of phase-contrast and fluorescent microscopy micrographs of untreated L929 fibroblasts (Ctrl); L929 fibroblasts incubated for 3 h at 37 °C in the presence of 2.5 μg/ml nocodazole (Noco); L929 fibroblasts incubated for 3 h at 37 °C in the presence of 2.5 μg/ml nocodazole and subsequently treated with PC for 2 min (Noco + PC); and L929 fibroblasts incubated for 3 h at 37 °C in the presence of 2.5 μg/ml nocodazole and 5 mM MβCD for 30 min at 37 °C and then treated with PC for 2 min (Noco + MβCD + PC). (B) Merge of DIC and fluorescent microscopy micrographs of platelets untreated (Ctrl) or treated with PC for 2 min (PC), with or without MβCD incubation (MβCD, MβCD + PC). The cells were fixed and the GM1 ganglioside was detected with biotin-conjugated cholera toxin B subunit and rhodamine-conjugated streptavidin (for fibroblasts) or fluorescein-conjugated streptavidin (for platelets) without permeabilization. Pictures are representative of the cells from three independent experiments. Scale bars, 10 μm.

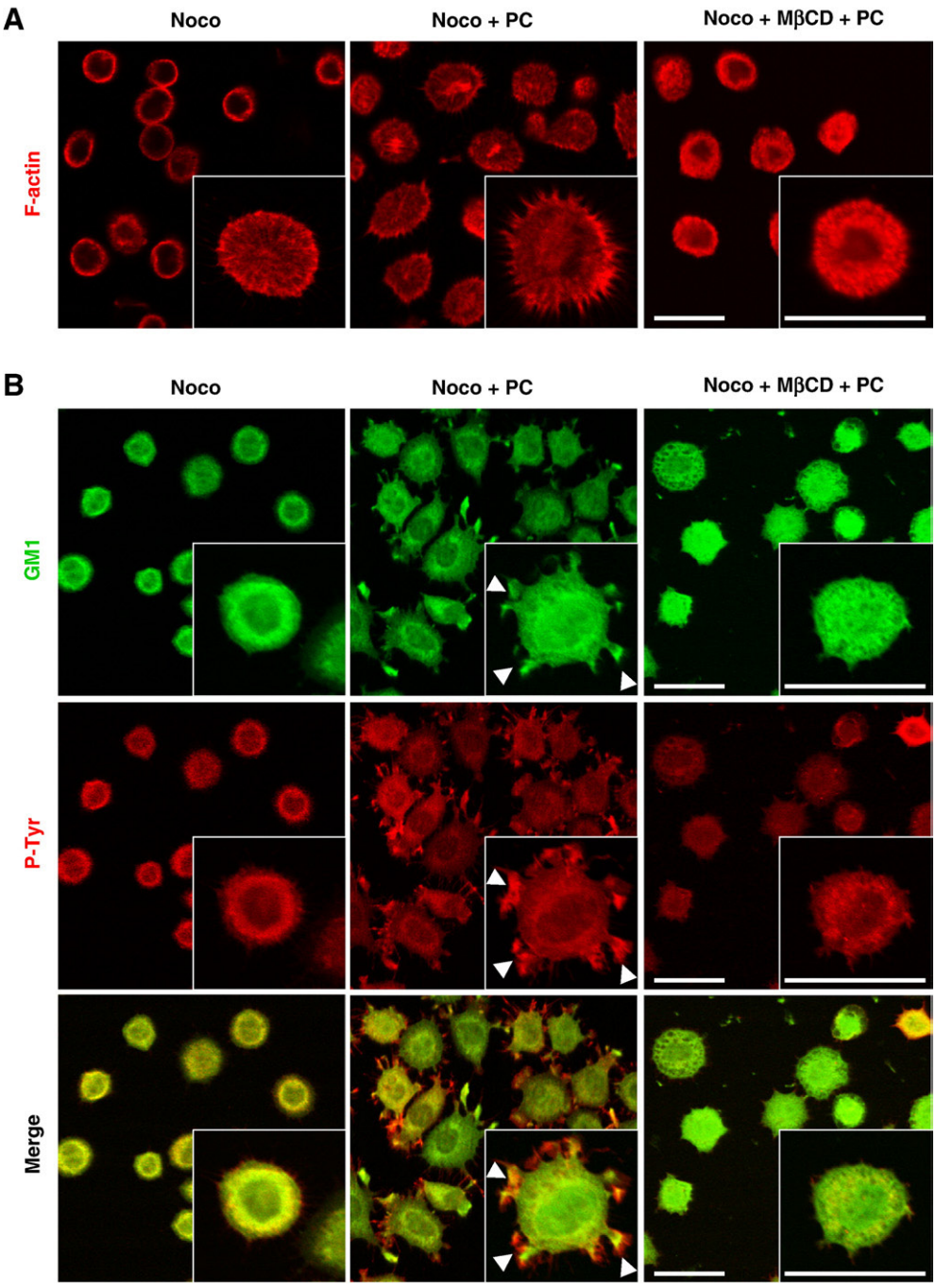

Fig. 3. Actin remodeling and tyrosine phosphorylation induced by phospholipid excess in fibroblasts. Confocal micrographs of L929 fibroblasts incubated for 3 h at 37 °C in the presence of 2.5 μg/ml nocodazole (Noco); L929 fibroblasts incubated for 3 h at 37 °C in the presence of 2.5 μg/ml nocodazole and subsequently treated with PC for 2 min (Noco + PC); and L929 fibroblasts incubated for 3 h at 37 °C in the presence of 2.5 μg/ml nocodazole and 5 mM MβCD for 30 min at 37 °C and then treated with PC for 2 min (Noco + MβCD + PC). (A) The cells were fixed and permeabilized and F-actin was labeled with phalloidin-TRITC. (B) Alternatively the GM1 ganglioside and the tyrosine-phosphorylated proteins were labeled, respectively, with cholera toxin B subunit-FITC and with the mouse monoclonal 4G10 anti-phospho-tyrosine antibody revealed with anti-mouse IgG-rhodamine. The arrowheads in the inset of panels Noco + PC indicate the co-localization of GM1 ganglioside and tyrosine-phosphorylated proteins. Pictures are representative of the cells from three independent experiments. Scale bars: 10 μm.

excess-driven cell shape changes and in the associated molecular events, such as actin polymerization and tyrosine phosphorylation.

3.4. Phospholipid excess in the outer leaflet induces the reversible enrichment of raft markers and tyrosine phosphorylation of several lipid raft proteins in resting platelets and fibroblasts

To evaluate the effects of the applied mechanical constraint on the outer leaflet of the plasma membrane of resting platelets and L929 fibroblasts at the biochemical level, we proceeded to a fractionation of the cells that were subjected to different treatments and isolated the DRM fractions containing lipid rafts. After incubation with a phospholipid excess, consisting of short-chain analogues of phospholipids (PS and PC), resting platelets (Fig. 4) and L929 fibroblasts (Fig. 5), depleted (with MβCD) or not (without MβCD) in cholesterol, were lysed after respectively 2 and 30 min of incubation with the phospholipid analogues. The different fractions obtained by ultracentrifugation on a sucrose gradient were analyzed for their content in raft

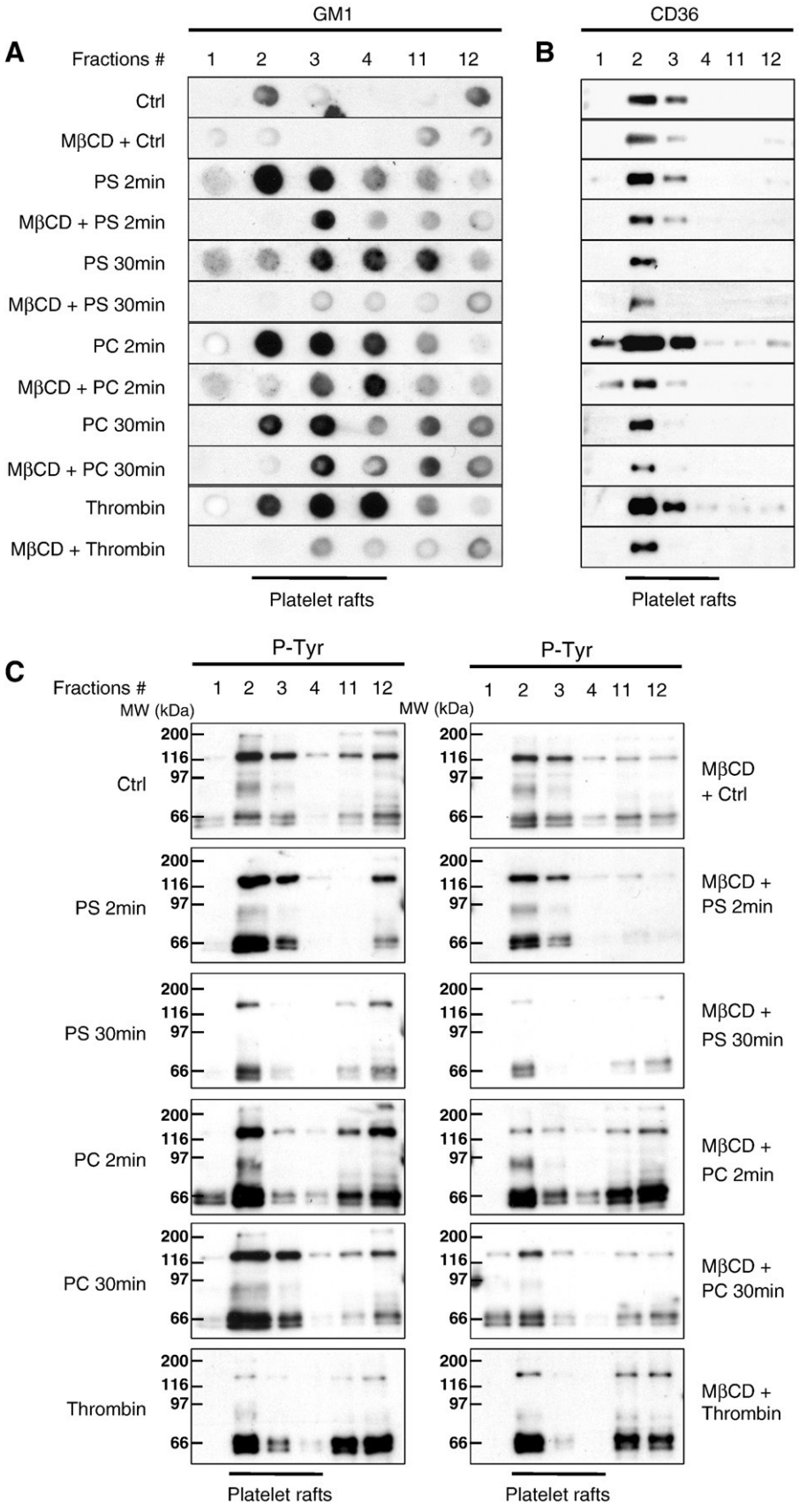

Fig. 4. Distribution of the raft markers and consequences of cholesterol depletion in platelets subjected to phospholipid excess. Platelets were incubated with excess phospholipids (PS or PC) pre-treated or not with MβCD. The raft and non-raft fractions were separated by a sucrose gradient equilibrium centrifugation of Triton X-100 platelet lysates. (A) Dot blot analysis of ganglioside GM1 distribution in separated fractions of lysed platelets under the indicated conditions of treatment. (B) Western blot analysis of CD36 distribution in separated fractions of lysed platelets under the same conditions of treatment as in A. (C) Western blot analysis of tyrosine-phosphorylated protein distribution in different fractions of lysed platelets under the indicated treatment conditions. Molecular weights are indicated on the left side of the blots. Data are representative of three independent experiments.

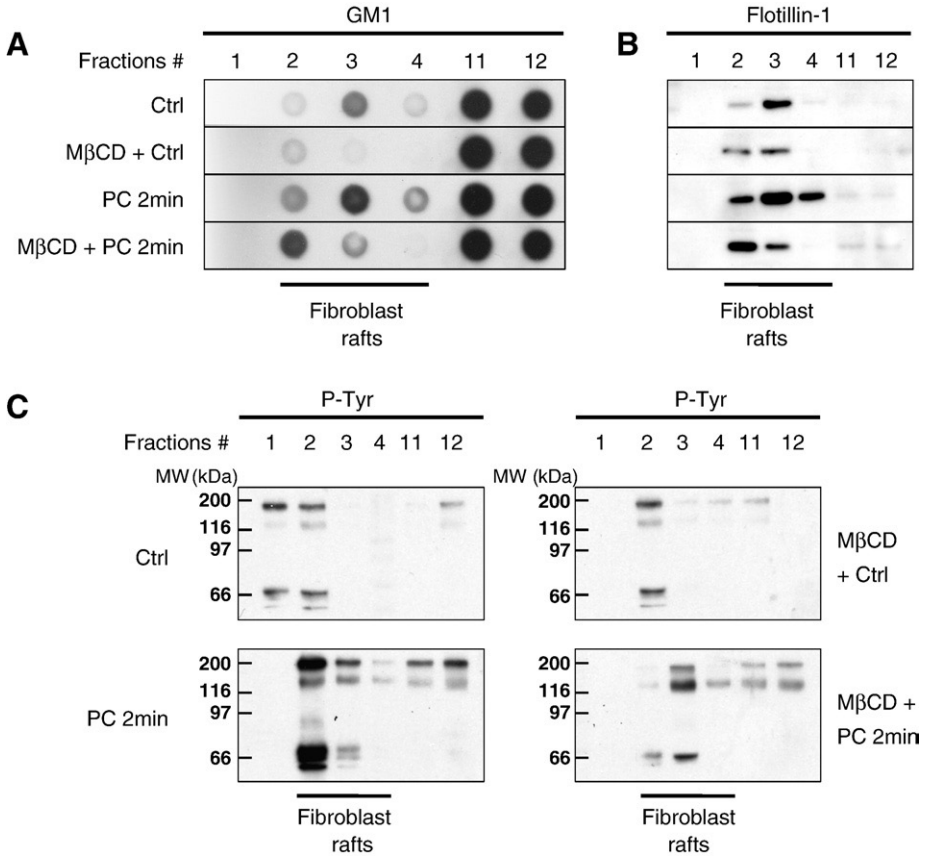

Fig. 5. Distribution of raft markers and consequences of the cholesterol depletion in L929 fibroblasts subjected to phospholipid excess. The fibroblasts were incubated with excess phospholipids (PC) pre-treated or not with MβCD. The raft and non-raft fractions were separated by a sucrose gradient equilibrium centrifugation of Triton X-100 fibroblast lysates. (A) Dot blot analysis of ganglioside GM1 distribution in separated fractions of lysed fibroblasts under the indicated treatment conditions. (B) Western blot analysis of flotillin-1 distribution in separated fractions of lysed fibroblasts under the same conditions of treatment as in A. (C) Western blot analysis of the tyrosine-phosphorylated protein distribution in separated fractions of lysed fibroblasts under the indicated treatment conditions. Molecular weights are indicated on the left side of the blots. Data are representative of three independent experiments.

markers (GM1 and CD36 for platelets in Fig. 4; GM1 and flotillin-1 for fibroblasts in Fig. 5) and in tyrosine-phosphorylated proteins (Figs. 4 and 5, P-Tyr). In Fig. 4A, the addition of phospholipid analogues (PS and PC) after 2 min of incubation induces enrichment of the ganglioside GM1 in raft fractions (Fig. 4A, PS 2 min and PC 2 min) and CD36 (Fig. 4B, PS 2 min and PC 2 min) as compared to untreated platelets (Figs. 4A and B, Ctrl). After 30 min incubation with the phosphatidylserine analogue, GM1 and CD36 are less enriched, demonstrating the reversibility of this process (Fig. 4A and B, PS 30 min). PS is known to be translocated to the inner leaflet by the aminophospholipid translocase, termed flippase [37]. Consequently, after 30 min incubation, the phospholipid excess in the outer leaflet does not persist. Conversely, GM1 is still enriched in the raft fractions after 30 min of incubation with the PC analogue (Fig. 4A, PC 30 min). For unknown reasons, CD36 is not maintained to the same extent as GM1 in these fractions (Fig. 4B, PC 30 min). As PC is not spontaneously translocated to the inner leaflet, the phospholipid excess in the outer leaflet of plasma membrane persists after 30 min. This demonstrates that the enrichment of GM1 in raft fractions requires a phospholipid excess in the outer leaflet of the membrane, which is persistent with phosphatidylcholine analogue treatment but reversible with phosphatidylserine analogue treatment. The cholesterol depletion by MβCD treatment abolishes this enrichment of GM1 and CD36 independent of the platelet treatment. As positive control, we used platelets activated by thrombin, which is known to enrich ganglioside GM1 and CD36 in the raft fractions (Fig. 4A and B, Thrombin) [38]. This enrichment was abolished by the depletion of cholesterol (Fig. 4A and B, MβCD + Thrombin). Furthermore, the mechanical constraint increases the tyrosine phosphorylation of proteins found in DRM fractions (Fig. 4C, PS 2 min, PC 2 min, PC 30 min and Thrombin). Interestingly, this enrichment is reversible when the phosphatidylserine analogue is added (Fig. 4C, PS 30 min), as it is translocated to the inner leaflet by the flippase [37] and is abolished by MβCD-cholesterol depletion (Fig. 4C). The bands exhibiting a decreased phosphorylation after thrombin treatment may be the consequence of the activation of protein tyrosine phosphatases. For example, the receptor-type protein tyrosine phosphatase B has been identified in the proteomic analysis after phospholipid addition (Table S1). The different phospho-tyrosine patterns obtained after thrombin and PL treatments most likely reflect the diverse signaling pathways activated by these treatments in platelets.

As in resting platelets, the addition of an excess of phospholipids to L929 fibroblasts induces enrichment of ganglioside GM1 and flotillin-1 to DRM fractions (Fig. 5A and B, PC 2 min) compared to the control cells (Fig. 5, Ctrl). The flotillin-1 enrichment is abolished when the fibroblasts were pre-treated with MβCD (Fig. 5B, MβCD + PC 2 min). The ganglioside GM1 level in the MβCD + PC-treated samples exhibits a 1.56-fold (SD<0.05) decrease as compared to PC, as quantified by densitometry (Image J, http://rsbweb.nih.gov/ij/) (Fig. 5A, MβCD + PC 2 min). Moreover, the mechanical constraint imposed to fibroblasts increases the tyrosine phosphorylation of the proteins of DRM fractions in a cholesterol-dependent manner (Fig. 5C). Taken together, these biochemical results indicate that a mechanical constraint applied to the plasma membrane of resting platelets and L929 fibroblasts triggers a reorganization of the membrane microdomains (enrichment of GM1, CD36 and flotillin-1 in DRM fractions) and an increase in tyrosine phosphorylation in a reversible manner.

These events are similar to those observed with thrombin-activated platelets. Cholesterol depletion reduces phospholipid excess-driven cell signaling showing that lipid raft integrity is necessary for sustaining the generated membrane extensions.

3.5. Proteomic analysis of the enriched DRM proteins from the resting platelets subjected to a phospholipid excess

To analyze the proteins enriched in lipid rafts after the addition of phospholipids to the outer leaflet of the platelet plasma membrane, the proteins in the light buoyant-density DRM fractions of resting human platelets incubated or not with a phospholipid excess and pre-treated or not with MβCD were pooled and separated by SDS–PAGE (Fig. 6A). The mechanical constraint generates a global protein enrichment in DRM fractions as illustrated by the Coomassie staining (Fig. 6A, PC). This enrichment is abolished by the depletion of cholesterol (Fig. 6A, MβCD + PC). The enriched protein bands were cut out and processed for identification by mass spectrometry (Fig. 6A, red arrowheads). Those displaying no increase in Coomassie staining were not analyzed (Fig. 6A, black arrowheads). To verify that this DRM

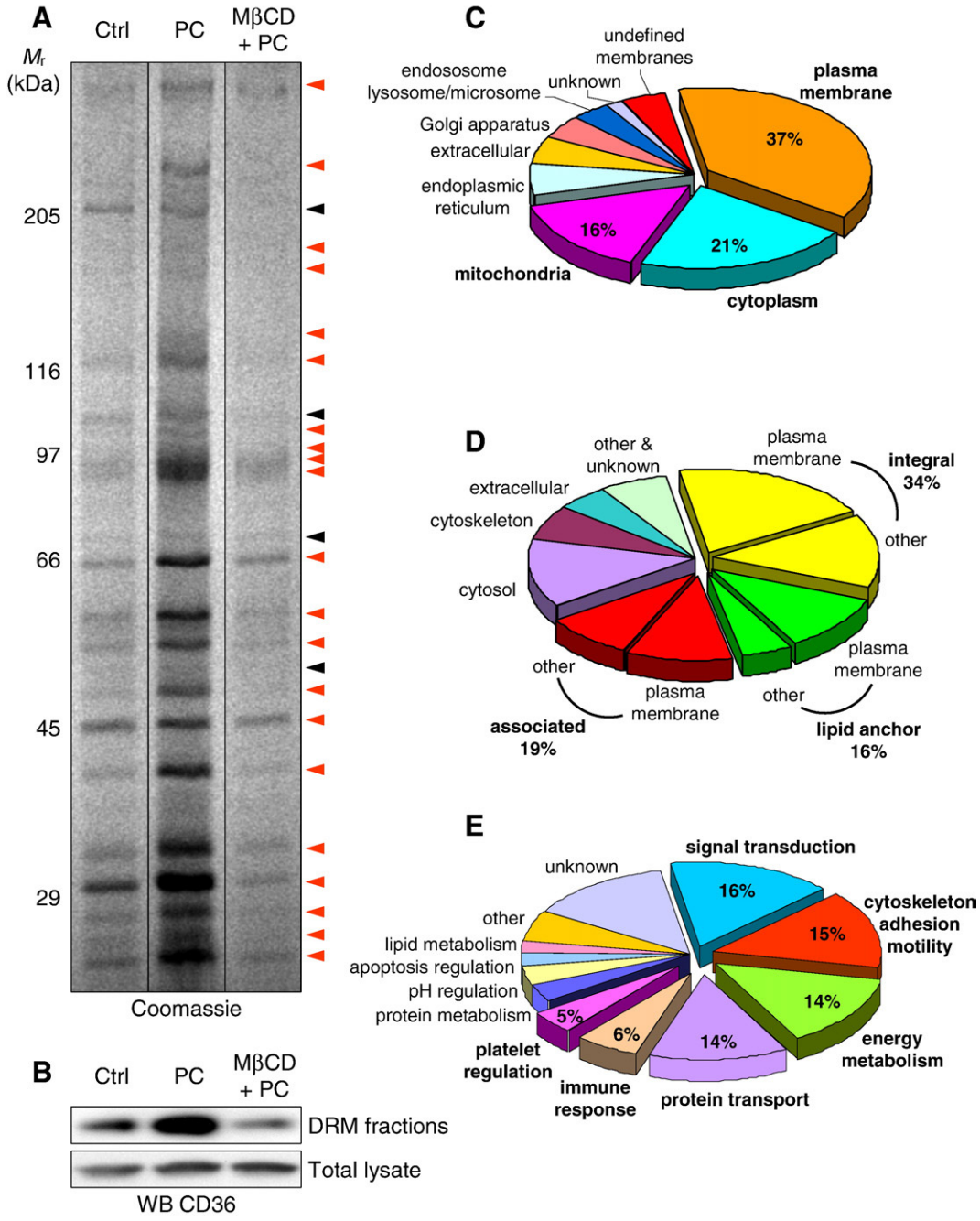

Fig. 6. Proteomic analysis of raft proteins in platelets subjected to a phospholipid excess. (A) The platelets were incubated or not with an excess of phospholipids (PC) and pre-treated or not with MβCD. The raft proteins were enriched by a sucrose gradient equilibrium centrifugation of Triton X-100 platelet lysates. The 4–15% gradient SDS–PAGE gel of pooled raft fractions obtained from the control platelets (Ctrl) and from the platelets subjected to phospholipid excess (PC) pre-treated or not with MβCD (MβCD + PC) was stained with Colloidal Blue. Protein bands enriched after PC incubation (red arrowheads) were cut out, digested by trypsin and analyzed by mass spectrometry. (B) CD36 distribution was analyzed by Western blot in DRM fractions and in total lysate. (C) Subcellular localization of raft proteins identified by mass spectrometry. (D) Molecular classification of identified raft proteins highlighting their association status with cellular membranes (integral, linked by a lipid anchor, associated or not with cellular membranes). (E) Biological processes in which identified raft proteins are involved.

protein enrichment is not due to changes in global protein contents, platelet proteins before (Fig. 6B, Total lysate) or after (Fig. 6B, DRM fractions) sucrose fractionation were subjected to SDS–PAGE and the presence of CD36 was analyzed by Western blot. In DRM fractions, CD36 is enriched after addition of phospholipid analogue (PC), depending on cholesterol depletion (PC + MβCD). In total lysates, CD36 presence is equal in all three conditions.

Using this methodology, we have identified 314 DRM-associated proteins. One hundred sixteen (37%) of the identified proteins are associated with the plasma membrane, 66 (21%) are cytoplasmic, 50 (16%) are mitochondrial and the remaining identified proteins are distributed within different organelles (Fig. 6C). The membrane proteins are distributed as follows: 34% are integral, 19% are membrane associated and 16% are lipid anchored (Fig. 6D). Concerning their function, 16% are involved in signal transduction, 15% in cytoskeleton, adhesion and motility, 14% in energy metabolism and protein transport, 6% in immune response and 5% in platelet regulation (Fig. 6E). The identified proteins include tyrosine kinases and platelets raft signaling proteins (e.g., fyn, lyn, src, LAT and flotillin), proteins associated with cellular extensions (e.g., Arp3, cdc42, rac1, rhoG and moesin), involved in cell adhesion (e.g., integrins alpha 6, beta 1 and 3 and vinculin) or platelet activation and blood coagulation (e.g., CD9, CD36, fibrinogen, glycoproteins 5, 6 and 9 and phospholipid scramblase 4) (Table 1). The complete list of identified proteins is detailed in the Table S1. The method we used does, however, not exclude the identification of certain non-raft specific proteins. Our analysis, however, reveals many proteins known to be associated with a raft "signature" (e.g., ephrin B1, flotillin-1 and -2, fyn/lyn/src, raftlin, LAT, LAT 2, CD36, CD9, PECAM-1, stomatin, Rab 11A, Ral-A, etc.) thereby comforting our results. Conversely, certain identified non-raft specific proteins (e.g., mitochondrial components) are clearly discernible. Interestingly, some of the enriched proteins (e.g., protein tyrosine kinases and cytoskeletal proteins) are related to the phospholipid excess-driven cell signaling, reinforcing the idea that lipid rafts are necessary to sustain the cellular extensions in response to a mechanical constraint.

Table 1
Listing of selected raft proteins in platelets subjected to phospholipids excess depending on their biological activities.

Protein name	SwissProt/TrEMBL accession number	Functional class
• Kinases and platelet raft signalisation proteins		
cAMP-dependent protein kinase type I-alpha regulatory subunit	P10644	Kinase (Ser/Thr)
fyn	P06241	Kinase (Tyr)
lyn	P07948	Kinase (Tyr)
Src	P12931	Kinase (Tyr)
LAT	O43561	Protein binding
LAT2	Q9GZY6	SH2 domain binding
Flotillin-1	O75955	Protein binding
Flotillin-2	Q14254	Protein binding
Raftlin	Q14699	Protein binding
• Proteins involved in cellular extensions		
Filamin alpha	P21333	Cytoskeletal protein
ARP3	P61158	Cytoskeletal protein
BASP1	P80723	DNA binding
CDC42	P60953	GTPase
rac1	P63000	GTPase
RhoG	P84095	GTPase
Rho, GDP dissociation inhibitor (GDI) beta	P52566	GTPase activator
Duet (kalirin Rho GEF isoform)	Q9Y2A5	GEF/kinase (Ser/Thr)
Coronin-1A	P31146	Cytoskeletal protein
Cortactin	Q14247	Cytoskeletal protein
Moesin	P26038	Cytoskeletal protein
Vasodilator-stimulated phosphoprotein	P50552	Cytoskeletal protein
• Proteins involved in cell adhesion		
PECAM 1	P16284	Adhesion molecule
Endothelial cell adhesion molecule	Q96AP7	Adhesion molecule
Ephrin B1	P98172	Adhesion molecule
Integrin alpha 6	P23229	Adhesion molecule
Integrin beta 1	P05556	Adhesion molecule
Integrin beta 3	P05106	Adhesion molecule
Junctional adhesion molecule A	Q9Y624	Adhesion molecule
Junctional adhesion molecule C	Q9BX67	Adhesion molecule
Unc-112-related protein 2 (Kindlin-3)	Q86UX7	Adhesion molecule
Plectin 1	Q15149	Cytoskeletal protein
Parvin beta	Q9HBI1	Cytoskeletal protein
Talin 1	Q9Y490	Cytoskeletal protein
vinculin	P18206	Cytoskeletal protein
RhoA	P61586	GTPase
• Proteins involved in platelet activation / blood coagulation		
CD36 (Platelet glycoprotein 4)	P16671	Protein binding
CD9 antigen (tetraspanin-29)	P21926	Protein binding
Fibrinogen alpha chain	P02671	Protein binding
Fibrinogen B beta chain	P02675	Protein binding
Glycoprotein 5	P40197	Protein binding
Glycoprotein 6	Q9HCN6	Collagen binding
Glycoprotein 9, platelet	P14770	Protein binding
Glycoprotein Ib alpha chain	P07359	Thrombin receptor
Glycoprotein Ib beta chain	P13224	Protein binding
Guanine nucleotide-binding protein G(q) alpha subunit	P50148	GTPase
Integrin alpha-IIb	P08514	Protein binding
Multimerin 1	Q13201	Secreted polypeptide
Phospholipid scramblase 4	Q9NRQ2	Scramblase
Platelet basic protein	P02775	Cytokine
Thrombospondin 1	P07996	Protein binding

4. Discussion

We have previously shown that the addition of a phospholipid excess to the outer leaflet of the plasma membrane of resting human platelets and mouse fibroblasts induces the formation of cellular extensions (filopodia and lamellipodia) and a reversible actin polymerization via phosphoinositide 3-kinase activation [15]. These data corroborate the relationship between the mechanical constraint acting on plasma membrane, cell shape changes and cytoskeleton reorganization [39].

Several studies demonstrated the implication of lipid rafts in various cellular processes such as protein sorting, signal transduction, endocytosis and phagocytosis. In the present study, we have investigated the function of lipid rafts as signaling platforms in response to a mechanical constraint induced by the addition of phospholipids to the outer leaflet of the plasma membrane of resting human platelets and mouse fibroblasts. Using MβCD, a cytochemical probe that binds selectively to cholesterol and disrupts cholesterol-rich microdomains, we provide evidence that lipid rafts are crucial to maintain the mechanical constraint and act as dynamic structures involved in the reorganization of the cytoskeleton and the formation of plasma membrane extensions. Cholesterol depletion impedes formation of cellular extensions and actin polymerization induced by a phospholipid excess in resting platelets (Fig. 1) and L929 fibroblasts (Figs. 2 and 3). These results reinforce the idea that lipid rafts participate actively in membrane dynamics and actin reorganization [40,41].

The relationship between a mechanical constraint applied to the plasma membrane and cell signaling remains, however, unknown. In this study, we showed that mechanical constraint induces protein tyrosine phosphorylation in the generated cellular extensions (Fig. 3) and in DRM fractions (Figs. 4 and 5). Moreover, the GM1 ganglioside raft marker accumulates in plasma membrane extensions generated by a mechanical constraint (Figs. 2 and 3). An excess of phospholipids induced an enrichment of raft markers such as ganglioside GM1, CD36 and flotillin-1 that is reversible [42–44]. When the mechanical constraint is maintained on the cell surface in the case of a phosphatidylcholine analogue treatment (that is not translocated by the aminophospholipid translocase to the inner leaflet of the plasma membrane), the recruitment of raft markers, the protein tyrosine

phosphorylation and the formation of plasma membrane extensions are prolonged. However, when the phospholipids are translocated to the inner leaflet, as after treatment with a phosphatidylserine analogue, these processes progressively disappear (Fig. 4). This reversibility highlights the predominant role of the mechanical constraint in these events. Together, our results suggest that the addition of phospholipids causes modulation of the plasma membrane lateral organization and raft protein tyrosine phosphorylation. The disruption of lipid rafts abolishes these processes, demonstrating that the integrity of lipid rafts is crucial for cell signaling in response to a mechanical constraint on the plasma membrane. Moreover, the same effects were obtained with platelets activated by thrombin, reinforcing the link between mechanical constraint and signaling.

The recruitment and concentration of lipid rafts underneath the plasma membrane extensions with specific enrichment of tyrosine phosphorylation are in agreement with the observation that accumulation of lipid rafts at the edge of spreading platelets, extended tips and filopodia in activated platelets coincides with the recruitment of c-Src, CD63 and integrins GPIbα and GPVI [23,45]. In this study, we investigated for the first time the recruitment and enrichment of proteins in platelet rafts under a mechanical constraint by a proteomic approach. The majority of proteins display enrichment in DRM fractions after the addition of phospholipids. This process requires lipid raft integrity as cholesterol depletion completely abolishes the increase of protein bands as judged by a Coomassie staining (Fig. 6). From the 314 identified proteins, a major part is implicated in signal transduction, cell adhesion and motility and formation of cell membrane extensions. Sixteen percent of the identified proteins are mitochondrial and are most likely artefacts from of the biochemical raft purification, as was observed also by Foster and collaborators [46]. However, more than 66% of the proteins are related to plasma membranes, either integral, lipid anchored or associated. Among these, the majority are described as plasma membrane proteins. We also observed the presence of proteins involved in signal transduction. The identified tyrosine kinases, signaling proteins and proteins associated with plasma membrane extensions could be related to the phospholipid excess-driven cell shape changes. Indeed, the recruitment of these signaling proteins could induce actin polymerization. Arp3 points toward the presence of the actin branching and nucleating Arp2/3 complex that could be activated by its binding to cortactin, a protein phosphorylated by Src family tyrosine kinases, thus regulating the formation of branched actin networks [47]. The Rho family GTPase Cdc42 could also indirectly regulate Arp2/3 [48]. The ERM protein moesin acts as a crosslinker between actin filaments and the plasma membrane via its interaction with PECAM 1 [49]. Another enriched protein is raftlin, which has been described as necessary for BCR signal transduction [50]. Furthermore, the identification of proteins involved in platelet activation and blood coagulation in mechanical-constrained platelets is in agreement with the results obtained with thrombin-activated platelets [38]. A remaining concern is to construct unambiguous models of protein behavior in lipid rafts and to discriminate between non-exclusive situations. For example, (i) proteins may already be localized in (small) lipid rafts of resting platelets and the mechanical constraint could induce coalescence of these small units, increasing the efficiency of their purification on a sucrose gradient. The tyrosine phosphorylation could then arise from kinases activated after a mechanical constraint and substrates already localized in the small lipid rafts of resting platelets. (ii) Lipid raft protein composition could be different between resting and constrained platelets and phospholipid excess could trigger a recruitment of specific proteins in lipid raft fractions. Tyrosine phosphorylation could induce an increase in the affinity between transient and permanent lipid raft proteins. This question could be addressed with a quantitative proteomic approach and will be the aim of future studies. Another crucial point concerns the distinction between of lipid/lipid versus protein/lipid and protein/protein interactions and inner versus outer leaflets of lipid bilayer membranes. In this study, we present biochemical evidence for a link between the mechanical constraints, the clustering of lipid rafts of the outer leaflet and the induction of signaling close to the inner leaflet of lipid rafts.

In conclusion, the morphological changes (filopodia and lamellipodia), the reversible actin polymerization and the activation of signaling proteins are associated with plasma membrane integrity, which is maintained by the cholesterol homeostasis. They are intimately linked with lipids rafts that are essential for the response to external forces. These observations support the notion that enrichment of tyrosine-phosphorylated proteins beneath the cellular extensions in response to a mechanical constraint is, at least in part, due to the integrity of lipids rafts. Our results not only strengthen the role of lipid rafts as signaling platforms but also as dynamic structures involved in the genesis of membrane extension in response to mechanical and external forces.

Acknowledgements

This study was supported by the Centre National de la Recherche Scientifique and the University of Montpellier II, the Institut National du Cancer (no.PL06-111 to PJ Coopman) and the Ligue Nationale contre le Cancer (LNCC; Equipe Labellisée Ligue 2007 to PJ Coopman). RM Larive is a recipient of a PhD fellowships funded by the LNCC and the Association pour la Recherche sur le Cancer (ARC). We gratefully acknowledge Michel Vidal, Stéphane Bodin and Andrea Parmeggiani for critically reading the manuscript, Alain Sahuquet for his help in image analysis. Image acquisitions were performed on workstations of the Montpellier RIO Imaging facility of MRI DBS-UM2. Mass Spectrometry experiments were carried out by using facilities of the Functional Proteomic Platform located at the Institut de Génomique Fonctionnelle (Montpellier, France).

Appendix A. Supplementary data

Supplementary data associated with this article can be found, in the online version, at doi:10.1016/j.bbamem.2009.11.016.

References

[1] M. Seigneuret, P.F. Devaux, ATP-dependent asymmetric distribution of spin-labeled phospholipids in the erythrocyte membrane: relation to shape changes, Proc. Natl. Acad. Sci. U. S. A. 81 (1984) 3751–3755.
[2] A. Suné, P. Bette-Bobillo, A. Bienvenüe, P. Fellmann, P.F. Devaux, Selective outside-inside translocation of aminophospholipids in human platelets, Biochemistry 26 (1987) 2972–2978.
[3] J. Kwik, S. Boyle, D. Fooksman, L. Margolis, M.P. Sheetz, M. Edidin, Membrane cholesterol, lateral mobility, and the phosphatidylinositol 4,5-bisphosphate-dependent organization of cell actin, Proc. Natl. Acad. Sci. U. S. A. 100 (2003) 13964–13969.
[4] J. Zimmerberg, M.M. Kozlov, How proteins produce cellular membrane curvature, Nat. Rev., Mol. Cell Biol. 7 (2006) 9–19.
[5] B.J. Peter, H.M. Kent, I.G. Mills, Y. Vallis, P.J. Butler, P.R. Evans, H.T. McMahon, BAR domains as sensors of membrane curvature: the amphiphysin BAR structure, Science 303 (2004) 495–499.
[6] T.H. Millard, G. Bompard, M.Y. Heung, T.R. Dafforn, D.J. Scott, L.M. Machesky, K. Futterer, Structural basis of filopodia formation induced by the IRSp53/MIM homology domain of human IRSp53, EMBO J. 24 (2005) 240–250.
[7] W.B. Huttner, J. Zimmerberg, Implications of lipid microdomains for membrane curvature, budding and fission, Curr. Opin. Cell Biol. 13 (2001) 478–484.
[8] F.A. Kuypers, X. Andriesse, P. Child, B. Roelofsen, J.A. Op den Kamp, L.L. van Deenen, The rate of uptake and efflux of phosphatidylcholine from human erythrocytes depends on the fatty acyl composition of the exchanging species, Biochim. Biophys. Acta 857 (1986) 75–84.
[9] M.P. Sheetz, R.G. Painter, S.J. Singer, Biological membranes as bilayer couples. III. Compensatory shape changes induced in membranes, J. Cell Biol. 70 (1976) 193–203.
[10] M.P. Sheetz, S.J. Singer, Biological membranes as bilayer couples. A molecular mechanism of drug-erythrocyte interactions, Proc. Natl. Acad. Sci. U. S. A. 71 (1974) 4457–4461.
[11] A. Schmidt, M. Wolde, C. Thiele, W. Fest, H. Kratzin, A.V. Podtelejnikov, W. Witke, W.B. Huttner, H.D. Soling, Endophilin I mediates synaptic vesicle formation by transfer of arachidonate to lysophosphatidic acid, Nature 401 (1999) 133–141.
[12] S.S. Vogel, E.A. Leikina, L.V. Chernomordik, Lysophosphatidylcholine reversibly arrests exocytosis and viral fusion at a stage between triggering and membrane merger, J. Biol. Chem. 268 (1993) 25764–25768.

[13] N. Bettache, P. Gaffet, N. Allegre, L. Maurin, F. Toti, J.M. Freyssinet, A. Bienvenue, Impaired redistribution of aminophospholipids with distinctive cell shape change during Ca^{2+}-induced activation of platelets from a patient with Scott syndrome, Br. J. Haematol. 101 (1998) 50–58.
[14] R.F. Zwaal, P. Comfurius, E.M. Bevers, Scott syndrome, a bleeding disorder caused by defective scrambling of membrane phospholipids, Biochim. Biophys. Acta 1636 (2004) 119–128.
[15] N. Bettache, L. Baisamy, S. Baghdiguian, B. Payrastre, P. Mangeat, A. Bienvenue, Mechanical constraint imposed on plasma membrane through transverse phospholipid imbalance induces reversible actin polymerization via phosphoinositide 3-kinase activation, J. Cell. Sci. 116 (2003) 2277–2284.
[16] E. Farge, D.M. Ojcius, A. Subtil, A. Dautry-Varsat, Enhancement of endocytosis due to aminophospholipid transport across the plasma membrane of living cells, Am. J. Physiol. 276 (1999) C725–733.
[17] H. Hagerstrand, M. Bobrowska-Hagerstrand, I. Lillsunde, B. Isomma, Vesiculation induced by amphiphiles and ionophore A23187 in porcine platelets: a transmission electron microscopic study, Chem. Biol. Interact. 101 (1996) 115–126.
[18] K. Simons, D. Toomre, Lipid rafts and signal transduction, Nat. Rev., Mol. Cell Biol. 1 (2000) 31–39.
[19] P.W. Janes, S.C. Ley, A.I. Magee, Aggregation of lipid rafts accompanies signaling via the T cell antigen receptor, J. Cell Biol. 147 (1999) 447–461.
[20] B.S. Wilson, S.L. Steinberg, K. Liederman, J.R. Pfeiffer, Z. Surviladze, J. Zhang, L.E. Samelson, L.H. Yang, P.G. Kotula, J.M. Oliver, Markers for detergent-resistant lipid rafts occupy distinct and dynamic domains in native membranes, Mol. Biol. Cell 15 (2004) 2580–2592.
[21] A.J. Garcia-Saez, S. Chiantia, P. Schwille, Effect of line tension on the lateral organization of lipid membranes, J. Biol. Chem. 282 (2007) 33537–33544.
[22] H. Hagerstrand, L. Mrowczynska, U. Salzer, R. Prohaska, K.A. Michelsen, V. Kralj-Iglic, A. Iglic, Curvature-dependent lateral distribution of raft markers in the human erythrocyte membrane, Mol. Membr. Biol. 23 (2006) 277–288.
[23] H.F. Heijnen, M. Van Lier, S. Waaijenborg, Y. Ohno-Iwashita, A.A. Waheed, M. Inomata, G. Gorter, W. Mobius, J.W. Akkerman, J.W. Slot, Concentration of rafts in platelet filopodia correlates with recruitment of c-Src and CD63 to these domains, J. Thromb. Haemost. 1 (2003) 1161–1173.
[24] N. Foger, R. Marhaba, M. Zoller, Involvement of CD44 in cytoskeleton rearrangement and raft reorganization in T cells, J. Cell. Sci. 114 (2001) 1169–1178.
[25] C.W. van den Berg, T. Cinek, M.B. Hallett, V. Horejsi, B.P. Morgan, Exogenous glycosyl phosphatidylinositol-anchored CD59 associates with kinases in membrane clusters on U937 cells and becomes Ca(2+)-signaling competent, J. Cell Biol. 131 (1995) 669–677.
[26] D.A. Brown, J.K. Rose, Sorting of GPI-anchored proteins to glycolipid-enriched membrane subdomains during transport to the apical cell surface, Cell 68 (1992) 533–544.
[27] D.J. Dorahy, G.F. Burns, Active Lyn protein tyrosine kinase is selectively enriched within membrane microdomains of resting platelets, Biochem. J. 333 (Pt. 2) (1998) 373–379.
[28] I. Stefanova, V. Horejsi, I.J. Ansotegui, W. Knapp, H. Stockinger, GPI-anchored cell-surface molecules complexed to protein tyrosine kinases, Science 254 (1991) 1016–1019.
[29] M. Kawabuchi, Y. Satomi, T. Takao, Y. Shimonishi, S. Nada, K. Nagai, A. Tarakhovsky, M. Okada, Transmembrane phosphoprotein Cbp regulates the activities of Src-family tyrosine kinases, Nature 404 (2000) 999–1003.
[30] F.H. Valone, E. Coles, V.R. Reinhold, E.J. Goetzl, Specific binding of phospholipid platelet-activating factor by human platelets, J. Immunol. 129 (1982) 1637–1641.
[31] P. Gaffet, N. Bettache, A. Bienvenue, Phosphatidylserine exposure on the platelet plasma membrane during A23187-induced activation is independent of cytoskeleton reorganization, Eur. J. Cell Biol. 67 (1995) 336–345.
[32] I. Kaverina, K. Rottner, J.V. Small, Targeting, capture, and stabilization of microtubules at early focal adhesions, J. Cell Biol. 142 (1998) 181–190.
[33] A. Suné, A. Bienvenüe, Relationship between the transverse distribution of phospholipids in plasma membrane and shape change of human platelets, Biochemistry 27 (1988) 6794–6800.
[34] I. Blikstad, F. Markey, L. Carlsson, T. Persson, U. Lindberg, Selective assay of monomeric and filamentous actin in cell extracts, using inhibition of deoxyribonuclease I, Cell 15 (1978) 935–943.
[35] J.E. Fox, M.E. Dockter, D.R. Phillips, An improved method for determining the actin filament content of nonmuscle cells by the DNase I inhibition assay, Anal. Biochem. 117 (1981) 170–177.
[36] A. Shevchenko, M. Wilm, O. Vorm, M. Mann, Mass spectrometric sequencing of proteins silver-stained polyacrylamide gels, Anal. Chem. 68 (1996) 850–858.
[37] P. Gaffet, N. Bettache, A. Bienvenue, Transverse redistribution of phospholipids during human platelet activation: evidence for a vectorial outflux specific to aminophospholipids, Biochemistry 34 (1995) 6762–6769.
[38] S. Bodin, C. Soulet, H. Tronchere, P. Sie, C. Gachet, M. Plantavid, B. Payrastre, Integrin-dependent interaction of lipid rafts with the actin cytoskeleton in activated human platelets, J. Cell. Sci. 118 (2005) 759–769.
[39] M.P. Sheetz, J. Dai, Modulation of membrane dynamics and cell motility by membrane tension, Trends Cell Biol. 6 (1996) 85–89.
[40] A. Vasanji, P.K. Ghosh, L.M. Graham, S.J. Eppell, P.L. Fox, Polarization of plasma membrane microviscosity during endothelial cell migration, Dev. Cell 6 (2004) 29–41.
[41] C. Gomez-Mouton, R.A. Lacalle, E. Mira, S. Jimenez-Baranda, D.F. Barber, A.C. Carrera, A.C. Martinez, S. Manes, Dynamic redistribution of raft domains as an organizing platform for signaling during cell chemotaxis, J. Cell Biol. 164 (2004) 759–768.
[42] P.E. Bickel, P.E. Scherer, J.E. Schnitzer, P. Oh, M.P. Lisanti, H.F. Lodish, Flotillin and epidermal surface antigen define a new family of caveolae-associated integral membrane proteins, J. Biol. Chem. 272 (1997) 13793–13802.
[43] D.J. Dorahy, L.F. Lincz, C.J. Meldrum, G.F. Burns, Biochemical isolation of a membrane microdomain from resting platelets highly enriched in the plasma membrane glycoprotein CD36, Biochem. J. 319 (Pt 1) (1996) 67–72.
[44] R.G. Parton, Ultrastructural localization of gangliosides; GM1 is concentrated in caveolae, J. Histochem. Cytochem. 42 (1994) 155–166.
[45] M. van Lier, F. Lee, R.W. Farndale, G. Gorter, S. Verhoef, Y. Ohno-Iwashita, J.W. Akkerman, H.F. Heijnen, Adhesive surface determines raft composition in platelets adhered under flow, J. Thromb. Haemost. 3 (2005) 2514–2525.
[46] L.J. Foster, C.L. De Hoog, M. Mann, Unbiased quantitative proteomics of lipid rafts reveals high specificity for signaling factors, Proc. Natl. Acad. Sci. U. S. A. 100 (2003) 5813–5818.
[47] B.L. Lua, B.C. Low, Cortactin phosphorylation as a switch for actin cytoskeletal network and cell dynamics control, FEBS Lett. 579 (2005) 577–585.
[48] H.N. Higgs, T.D. Pollard, Regulation of actin filament network formation through ARP2/3 complex: activation by a diverse array of proteins, Annu. Rev. Biochem. 70 (2001) 649–676.
[49] M.-A. Gamulescu, K. Seifert, M. Tingart, H. Falet, K.M. Hoffmeister, Platelet moesin interacts with PECAM-1 (CD31), Platelets 14 (2003) 211–217.
[50] K. Saeki, Y. Miura, D. Aki, T. Kurosaki, A. Yoshimura, The B cell-specific major raft protein, Raftlin, is necessary for the integrity of lipid raft and BCR signal transduction, EMBO J. 22 (2003) 3015–3026.